Available online at www.sciencedirect.com
ScienceDirect
Journal of Applied Geophysics 61 (2007) 56–81
JOURNAL OF APPLIED GEOPHYSICS
www.elsevier.com/locate/jappgeo

Joint inversion of surface wave dispersion curves and reflection travel times via multi-objective evolutionary algorithms

G. Dal Moro*, M. Pipan

Department of Geological Environmental and Marine Sciences (DiSGAM), University of Trieste, Via Weiss 1, 34100 Trieste, Italy

Received 30 September 2005; accepted 7 April 2006

Abstract

Due to the character of seismic energy generation and propagation, shallow high-resolution seismic-reflection surveys often fail in the identification of the shallowest horizons and, due to the limited offsets, accuracy of velocity analyses is often not very high.

In recent years, Rayleigh wave dispersion analysis have proved to have good potential also for near-surface applications but dispersion curve inversion and related uncertainty evaluation pose serious problems to a completely stand-alone application.

In order to overcome these problems a joint inversion scheme is proposed, which is based on the identification of the Pareto front, performed in the framework of a Multi-Objective Evolutionary Algorithm (MOEA). Seismic data considered to design the two objectives are the Rayleigh wave dispersion curve and reflection travel times.

We initially analyse a set of synthetic cases and evaluate the obtained results. A significant improvement of the retrieved models is observed as long as reflection travel times are added to the dispersion curve alone.

Furthermore, the proposed methodology also provides relevant indications about the consistency of the overall inversion process. In fact, the distribution of the models in the objective space, the trend of the objectives over the passing generations and the evolution of the Pareto front can provide useful information to evaluate the provisional tentative interpretation (number of strata and reflector identification) inherently adopted for the data inversion.

On the basis of the results obtained from the tests on the synthetic datasets, the analyses of a field dataset are interpreted as possible evidence of lateral heterogeneities.

Keywords: Joint inversion of seismic data; Multi-objective problems; Genetic algorithms; Pareto front; Surface wave dispersion; Shear-wave reflection

1. Introduction

Seismic energy generation mechanisms produce a non-uniform partition of energy among the different wave field components. If we consider a perfectly homogeneous medium and a vertically incident force on the free surface, surface waves (in this case just Rayleigh's) account for approximately 67% of the total energy while the rest is distributed into shear- (about 26%) and compressional-waves (only 7%) (e.g. Woods, 1968).

Shallow reflection seismic surveys are further made difficult because of various other phenomena: the coexistence of several components (surface and guided waves, refractions and diffractions etc.), near-field effects, the limited spectral band of the source and the

* Corresponding author. Tel.: +39 040 5582287; fax: +39 040 5582290.
E-mail address: dalmoro@units.it (G. Dal Moro).

0926-9851/$ - see front matter © 2006 Elsevier B.V. All rights reserved.
doi:10.1016/j.jappgeo.2006.04.001

frequency loss due to attenuation phenomena, misinterpretation on processed data of refractions and airwaves as reflectors and the possible appearance of processing artefacts.

All these data and phenomena explains why shallow high-resolution reflection surveys represent a very challenging task and why the shallowest horizons are typically very hard to image (Steeples and Miller, 1998).

It must be also underlined that the reliability of near-surface image purely based on reflection data can have imprecise results also because, due to the limited offsets, the accuracy of the velocity analyses is often not very high.

Over the last decade it has been shown that surface wave dispersion analysis can provide a crucial tool to reconstruct the vertical shear-wave profile (Glangeaud et al., 1999; Park et al., 1999; Xia et al., 1999, 2003, 2004; Dal Moro et al., in press-a) even if some problematic aspects probably prevent this investigation tool from being a fully stand-alone technique.

Dispersion curve inversion is in fact a highly nonlinear and multimodal problem that severely challenges any inversion procedure and necessarily holds an intrinsic indeterminacy which results particularly challenging especially if we consider that the proper number of strata to consider is actually unknown (Dal Moro et al., in press-b).

In addition, as the acquisition arrays are typically few tens-of-meters long (e.g. 24 2 m-spaced geophones, so a 46 m-long array) and the inversion is performed by considering a 1D Earth model, further problems can arise because of lateral heterogeneities.

This scenario makes apparent the importance of a robust joint inversion scheme able to take advantage of both the techniques (reflection surveys and dispersion curve analysis) and overcome the intrinsic limitations of each method.

The fundamental aspect that characterizes the problem is that the two phenomena/datasets are deeply different in terms of physical quantities they consider (such objectives are said to be *non-commensurable*) and many common joint inversion procedures would hardly handle different quantities unless inelegant and tricky solutions to normalize and sum up the data are applied.

Previous attempts to jointly exploit surface wave dispersion curve and reflection data for a marine dataset have been for example addressed via single penalty function evaluation (Ritzwoller and Lavshin, 2003) but, as previously mentioned, one of the main problems with single-objective optimisers is due to the necessity of combining the various objective functions into a single value according to an arbitrary sum of the adopted objectives.

It must be noticed that when a penalty function is defined according to a summation of single quantities, problems can arise when the single functions are in conflict. While this is very common for instance in economical problems or production applications, in geophysical data inversion this can occur when we consider the natural uncertainties that affect the data but, as the present work will show, can also play a crucial role in data analysis and inversion, furnishing the user a powerful tool that can prevent erroneous data interpretations.

The ensemble of these considerations led us into the Pareto front (PF) analysis that we considered in the framework of a Multi-Objective Evolutionary Algorithm (MOEA).

We considered the bi-objective problem determined by the use of the Rayleigh wave dispersion curves (our first objective) and the reflection travel times (the second objective) and designed a Matlab toolbox (*SeismoPareto*) on the basis of an Evolutionary Multi-Objective routine by Whidborne et al. (1994).

Shear-wave travel times (e.g. Tatham and McCormack, 1991) were adopted for the second objective. SH-wave surveys can provide good results even in situations where ordinary P-wave analyses are often unsuccessful because of a poor signal-to-noise ratio (e.g. Guy et al., 2003; Dal Moro et al., 2005) and allow a stricter link with the dispersion curve, being the Rayleigh wave propagation determined by V_S rather than V_P (e.g. Xia et al., 1999).

The paper is composed of four main sections: a description of the methodology, a presentation of the analyses performed both for synthetic and real datasets, a discussion of the results and a concluding paragraph.

2. The methodology

In disciplines like economy, production and engineering applications, game theory and artificial intelligence, problems involving several often-conflicting (or even independent) objectives are quite common and the need for rigorous and quantitative methods for determining the *best* solutions for a given Multi-Objective Problem (MOP) dates back to the end of the XIX century with the pioneering works of Edgeworth and Pareto. They defined a criterion to identify a set of optimal solutions based on *dominance* with respect to the rest of the possible solutions. Several good introductory publications are available on the subject (Van Veldhuizen

and Lamont, 1998a; Zitzler and Thiele, 1999; Van Veldhuizen and Lamont, 2000; Coello Coello, 2002, 2003) and we will therefore give only basic definitions to describe the methodology adopted for the present work.

A vector $\vec{u} = (u_1, u_2, \ldots, u_k)$ is said to dominate $\vec{v} = (v_1, v_2, \ldots, v_k)$ if and only if $\vec{u}$ is partially less than $\vec{v}$, that is

$$\forall i \in \{1, \ldots, k\}, u_i \leq v_i \wedge \exists i \in \{1, \ldots, k\} : u_i < v_i \quad (1)$$

where k represents the number of considered objective functions.

A solution $x \in \Omega$ (the decision variable space) is said to be the *Pareto optimal* with respect to the universe Ω if and only if there is no $x' \in \Omega$ for which $\vec{v} = F(x')$ dominates $\vec{u} = F(x)$.

For a given MOP the ensemble of undominated solutions define the *Pareto optimal set* P while the *Pareto front* PF is then defined as

$$\mathrm{PF} := \{\vec{u} = F(x) = (f_1(x), \ldots, f_k(x)) | x \in P\}. \quad (2)$$

An example of the Pareto front for a bi-objective problem (easy to be graphically represented in a Cartesian reference system) is reported in Fig. 1. The solutions belonging to the Pareto front are such that no improvement in one objective function can be achieved without producing a simultaneous degradation in at least one of the other objectives. In such a way we are able to measure how *good* is a solution x (in our case a certain Earth model) with respect to the other candidate solutions (other possible Earth models).

This approach was considered in the framework of an optimization scheme based on a genetic algorithm.

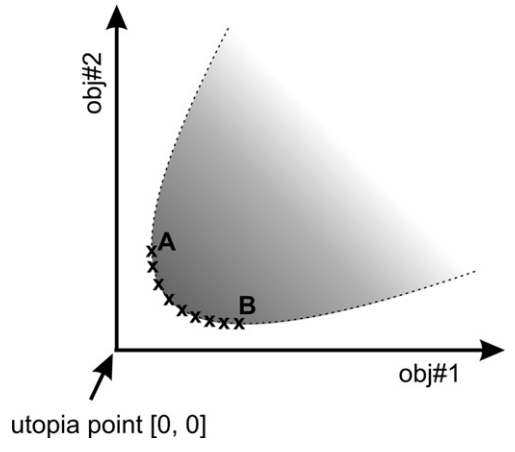

Fig. 1. Pareto front (models marked by crosses along the A–B arc) for a bi-objective problem.

In fact, a ranking process can be adopted in order to identify the *fittest* models and proceed with the optimization procedure through the application of the genetic operations of *selection crossover* and *mutation*.

The method adopted to define the rank of a given model is based on the number of individuals that are dominated by it, basically according to the dominance criterion reported in Eq. (1).

At the generation t, the rank of the individual x_i (a candidate solution) is then determined as:

$$\mathrm{rank}(x_i, t) = 1 + p_i^{(t)} \quad (3)$$

where the quantity $p_i^{(t)}$ represents the number of individuals that dominate x_i — see Fonseca and Fleming (1993) for further details.

Once the rank is established, the *fitness* is then calculated according to a function that spans from the best (rank = 1) to the worst (rank $\leq N$) values, where N represents the population size. *Selection*, *crossover* and *mutation* procedures are then performed according to common genetic procedures [see e.g. Goldberg (1989) and Man et al. (2001) for an introduction to Evolutionary Algorithms (EA)].

In short, once an initial random population is generated, the method consists of two main processes:

1) A decision step aimed at determining the best individuals of a given generation. This is accomplished through the identification of the non-dominated solutions, their ranking and subsequent fitness assignment;
2) Application of the genetic procedures to the individuals selected according to the above-mentioned procedure.

The application of such operations is performed for a number of times (generation number) specified by the user or till a certain criterion/requirement is met.

For a given MOP, it is particularly remarkable that an EA using a Pareto-based ranking system (and a monotonic selection algorithm such those based on a Pareto-based fitness assignment) tends to converge to the global optimum represented by the Pareto front PF (Van Veldhuizen and Lamont, 1998b).

In terms of probability this can be expressed as

$$P\{\lim_{t \to \infty} \mathrm{PF} \in P(t)\} = 1 \quad (4)$$

where $P(t)$ is the current (i.e. "temporary" or "local") set of Pareto solutions.

It must be clearly remarked that, unlike single objective optimizations, in MOP the solution is usually

Table 1
Parameters of the synthetic models: V_S is the shear-wave velocity (m/s), ρ the density (g/cm^3) and THK the thickness (m)

		Model#1			Model#2		
		V_S (m/s)	ρ (g/cm^3)	THK (m)	V_S (m/s)	ρ (g/cm^3)	THK (m)
Layer	1	130	1.78	3.6	150	1.7	3.0
	2	177	1.85	4.7	177	1.7	5.3
	3	119	1.76	4.2	119	1.7	4.2
	4	400	1.98	5.6	400	1.8	5.6
	5	2000	2.36	∞	2000	2.4	∞

V_P values (not listed for the sake of brevity) are defined according to Poisson's ratio values equal to 0.4 when $V_S \leq 400$ m/s, 0.3 for $400 < V_S \leq 1500$ and 0.25 for $V_S > 1500$. Density values ρ fixed according to Eq. (9).

not single but rather a set of *good* solutions referred to as the Pareto optimal.

2.1. The objective functions

The two objective functions we considered are defined as the *root–mean–square* (*rms*) misfit (the ℓ2-norm) between the observed and calculated dispersion curves (first objective, hereafter obj#1) and the reflection travel times (second objective, hereafter obj#2):

$$\text{obj} = \sqrt{\frac{\sum_{i=1}^{n} (\phi_{\text{obs}_i} - \phi_{\text{cal}_i})^2}{n}} \tag{5}$$

where Φ represents the Rayleigh-wave phase velocities (obj#1) or the reflection travel times (obj#2) and n is the number of observations for the given objective.

Table 2
Genetic parameters adopted for the performed inversions

Population size	50
Crossover rate	0.7
Mutation rate	0.1
Number of generations	150
Crossover type	Intermediate recombination
Selection type	Roulette wheel selection
Selection pressure	1.5

As far it concerns the obj#1, the ith misfit (at frequency f_i) is multiplied by a factor w_i calculated as:

$$w_i = \sqrt{\frac{f_i}{f_M}} \tag{6}$$

where f_M represents the maximum frequency of the considered dispersion curve.

Such weighting procedure aims at avoiding that the higher misfits occurring at lower frequencies dominate over the smaller misfits at higher frequencies (thus possibly determining a loss of resolution for the shallowest layers).

The dispersion curve forward modelling was calculated according to Lai and Rix (1998) while for the calculation of the reflection travel times we adopted the CREWES Project routine (AAVV, 2001).

For the present work it can be noticed that

$$\text{obj\#1} = f(V_S, \text{THK}, \rho, V_P) \tag{7}$$

$$\text{obj\#2} = f(V_S, \text{THK}) \tag{8}$$

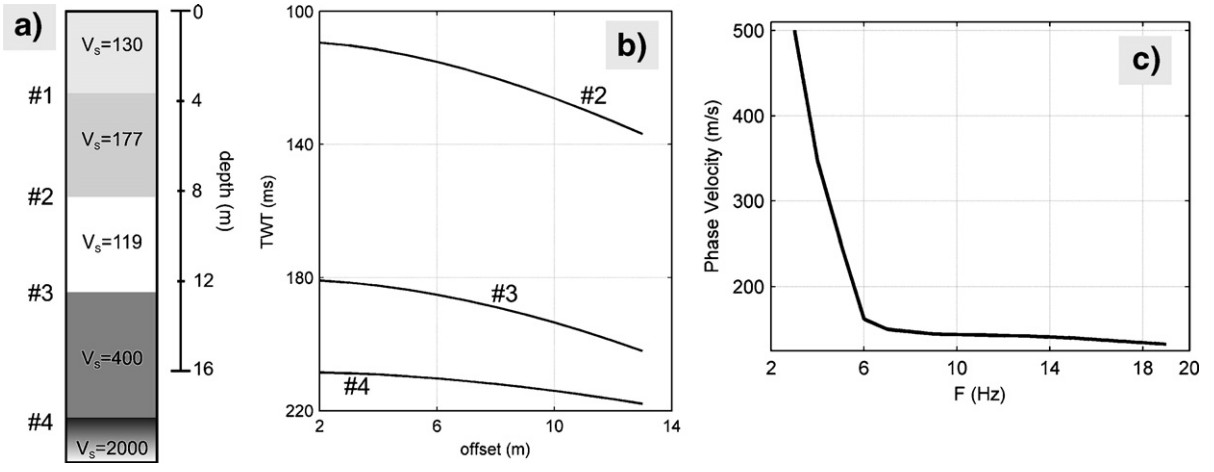

Fig. 2. Synthetic model#1 (see Table 1) together with the S-wave reflection travel times of the indicated horizons and the dispersion curve.

Table 3
Search space adopted for the performed inversions

Layer	V_S (m/s)	THK (m)
1	90÷200	1÷5
2	90÷300	2÷7
3	90÷300	3÷7
4	200÷700	3÷7
5	1000÷2500	half-space

where V_S and V_P are the shear- and compressional-wave velocities, THK the thickness and ρ the density.

3. Data inversions

The most important parameters that influence the Rayleigh wave propagation are the shear-wave velocity and layer thickness, while density ρ and P-wave velocity play a minor role (Xia et al., 1999). Therefore, in order to reduce the computational load and the degree of freedom of the system, only the first two parameters were considered as variables. Compressional-wave velocities were fixed on the basis of the shear-wave velocities according to Poisson's values proportional to V_S: 0.4 when $V_S \leq 400$ m/s, 0.3 for $400 < V_S \leq 1500$ and 0.25 for $V_S > 1500$ (Ivanov et al., 2000; Adme, 2004).

The classical Gardner et al. (1974) empirical V_P–ρ relationship was then used to fix the density values:

$$\rho = \log(0.23 + (kV_P)^{0.25}) \tag{9}$$

where $k = 1/0.3048$ is a constant to convert feet into meters.

The results of some tests performed on a synthetic dataset (model#1 in Table 1 and Fig. 2) are analysed in order to illustrate some paradigms useful in the discussion of the results obtained for a field dataset.

We performed data inversions by considering the genetic parameters reported in Table 2. As also observed by Sen and Stoffa (1992) it is however noticeable that moderate variations of the adopted genetic functions and parameters scarcely influence the performances of the algorithm (see also Dal Moro et al., in press-b).

In order to simulate a realistic situation in which there is a limited *a priori* knowledge about the site, we intentionally set a very wide search space (also known as *parameter space*) (Table 3).

For the tests on the synthetic data, to define the goodness-of-fit for a retrieved model with respect to the real one, a *Similarity Index* (SI) was adopted:

$$\mathrm{SI} = \left(1 - \frac{\sum_{i=1}^{n} \frac{|P_i^r - P_i^m|}{P_i^r}}{n}\right) 100 \tag{10}$$

where P_i^r and P_i^m are the considered variables (in the present case V_S and thickness) for the real and retrieved model, respectively and n is the total number of considered variables. When the two models are perfectly equal SI reaches a value of 100% clearly

Table 4
Tests performed on the synthetic dataset: test identification number, used objectives and Similarity Index (SI) for the retrieved models (in parentheses the minimum and maximum SIs for the Pareto front population)

	Test	Objectives	SI (%)
	#1	obj#1 (dispersion curve only)	*Best* mod.: 75.2 *Mean* mod.: 75.4
	#2	obj#1 + obj#2 (only reflector#3)	85.0 (77.6 - 86.5)
	#3	obj#1 + obj#2 (reflectors# 2, 3 and 4)	87.7 (86.9 - 89.5)
Erroneous assumptions	#4	obj#1 + obj#2 (reflector#4 wrongly assumed as #3)	76.7 (71.7 - 82.6)
Erroneous assumptions	#5	obj#1 + obj#2 (reflector#4 wrongly assumed as #2)	63.5 (55.7 - 85.2)
Erroneous assumptions	#6	obj#1 + obj#2 (two properly-interpreted deep reflectors with erroneous number of strata)	79.9 (75.3 - 85.0)
Erroneous assumptions	#7	obj#1 + obj#2: different models for the dispersion curve (model#1) and reflection travel times (model#2)	to model#1: 84.2 (80.4 - 86.1) to model#2: 87.3 (84.3 - 88.6)

decreasing as much as the retrieved model differs from the real one.

A mean model and its standard deviations were calculated according to the *Marginal Posterior Probability Density* (MPPD) (e.g. Frazer and Basu, 1990; Stoffa and Sen, 1991; Sen and Stoffa, 1992; Gerstoft and Mecklenbrauker, 1998; Dal Moro et al., in press-b), in order to define a unique model out of the set of Pareto optimal solutions, even if the limited number of models can decrease the statistical significance of such operation.

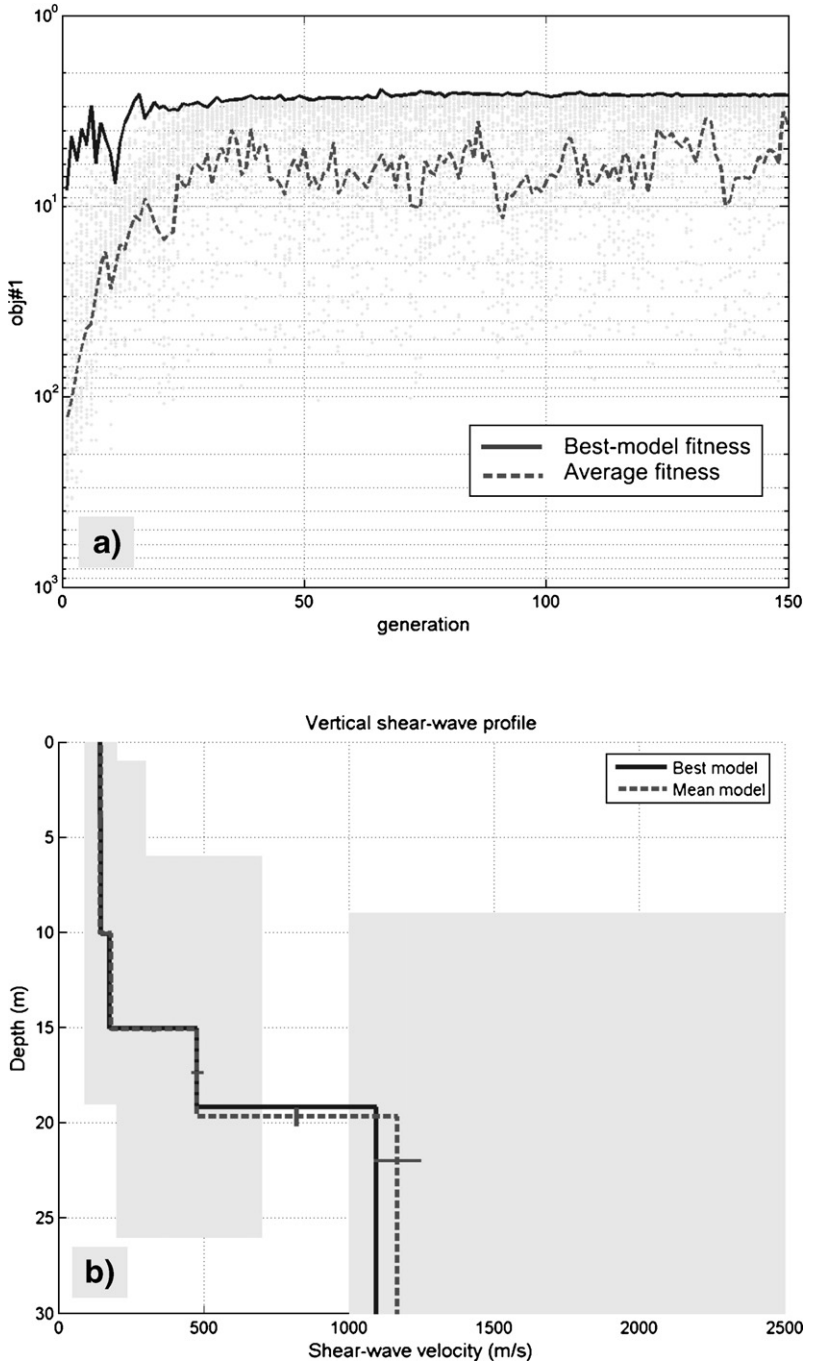

Fig. 3. Synthetic case: single-objective inversion (test#1): (a) dispersion curve misfit (obj#1) versus generation, (b) retrieved models (in light grey the search space).

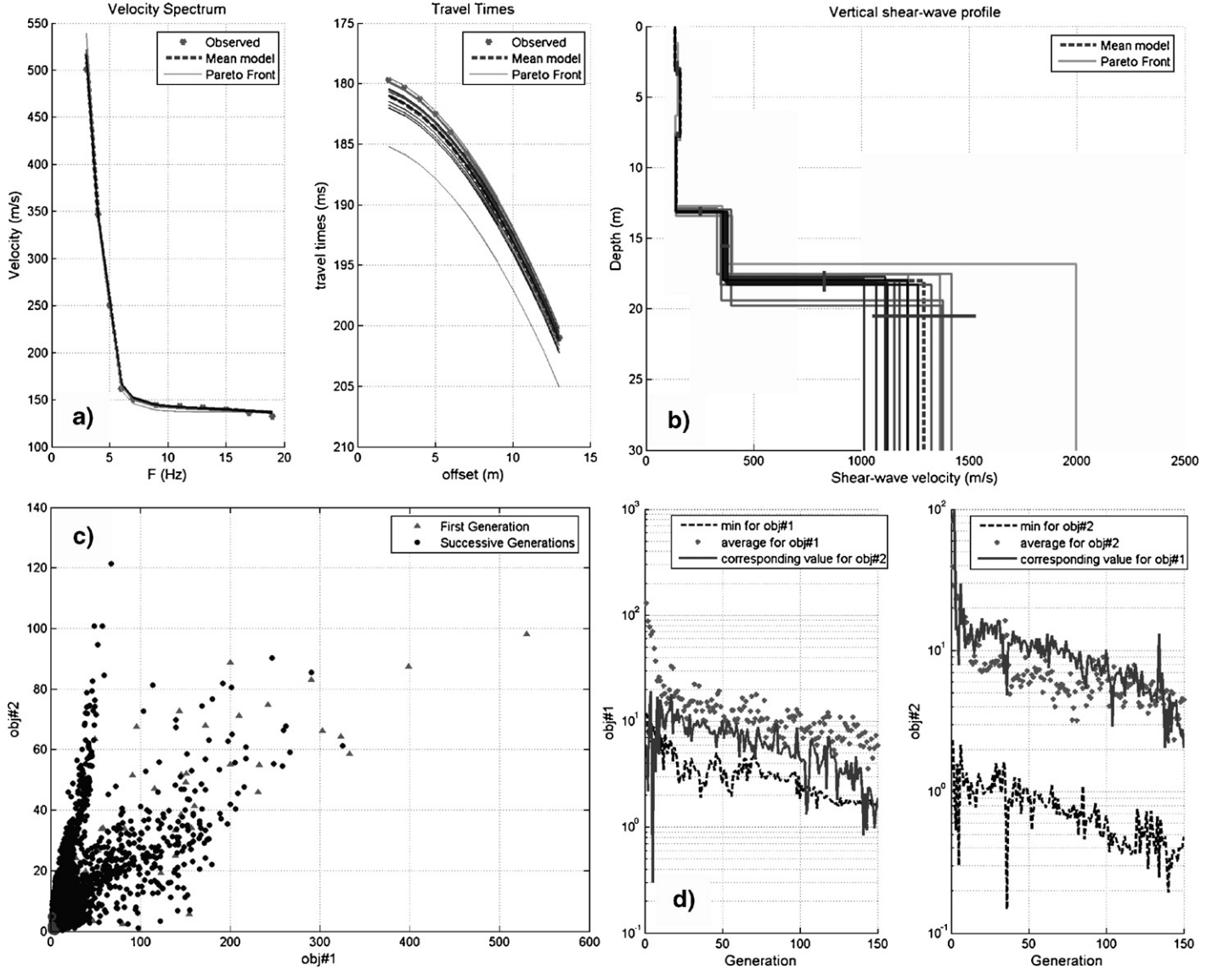

Fig. 4. Synthetic case, test#2: (a) observed and calculated data (mean and Pareto front models), (b) retrieved models, (c) objective space and (d) objective evolution over the generations.

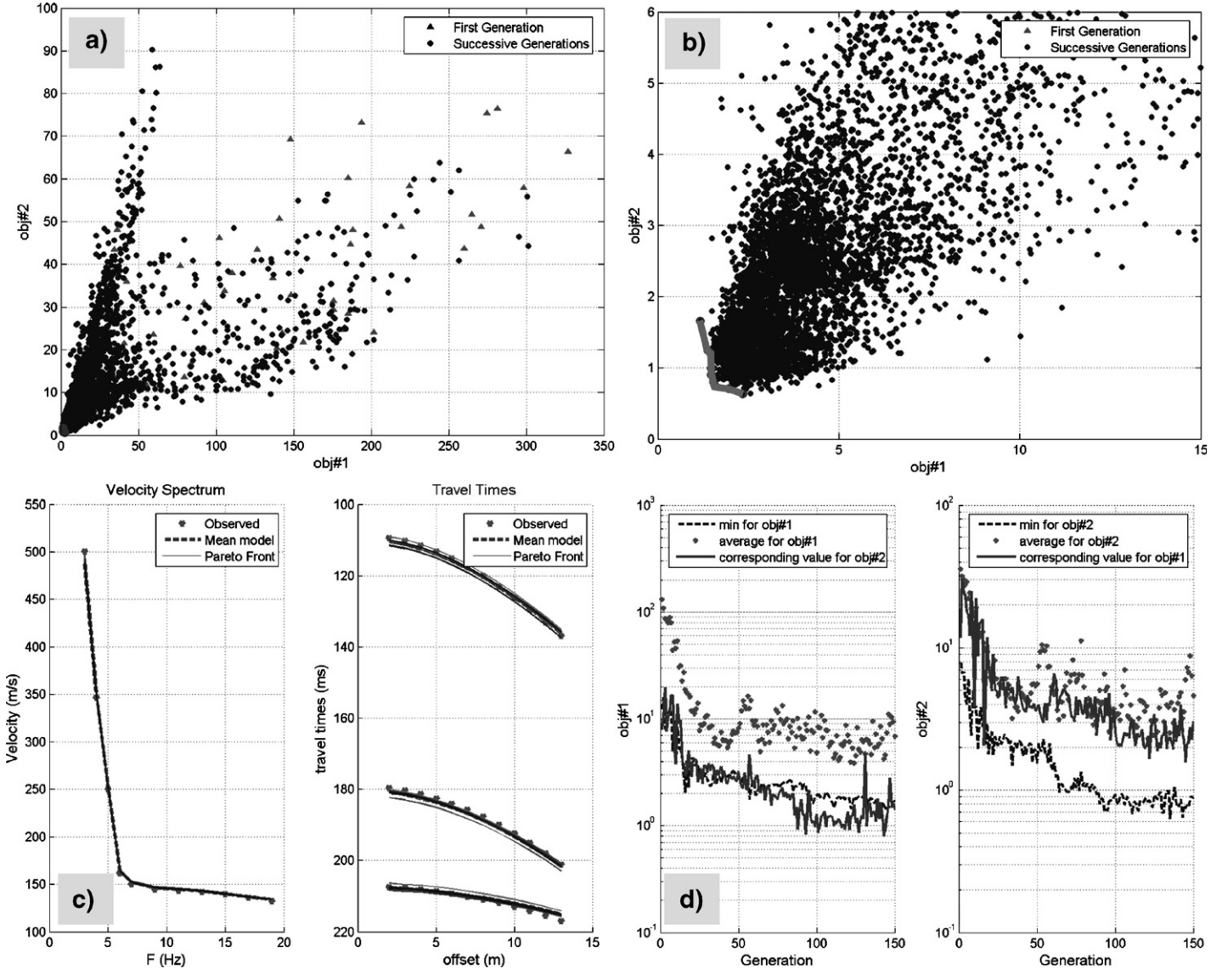

Fig. 5. Synthetic case, test#3: (a) objective space, (b) zoom of the Pareto front region (also indicated the approximate length of the Pareto front), (c) observed and calculated data (mean and Pareto front models), (d) objective evolution over the generations.

As a general statistical definition, the *a posteriori* mean model is determined according to

$$\langle m \rangle = \int dm\, m\, \sigma(m) \tag{11}$$

where $\sigma(m)$ represents the joint posterior probability density defined as

$$\sigma(m) = \frac{e^{E(m)}}{\sum e^{E(m)}} \tag{12}$$

where the value used as expectation $E(m)$ is the average of the values of the two objective functions (normalized in order to account for their non-commensurable nature).

The models considered for the summation are those belonging to the Pareto front (the set of the non-dominated solutions with rank equal to 1) and because of the limited number of individuals the mean value can be simply considered as a kind of average solution "weighted" according to Eq. (12). Standard deviations are calculated by considering the square roots of the

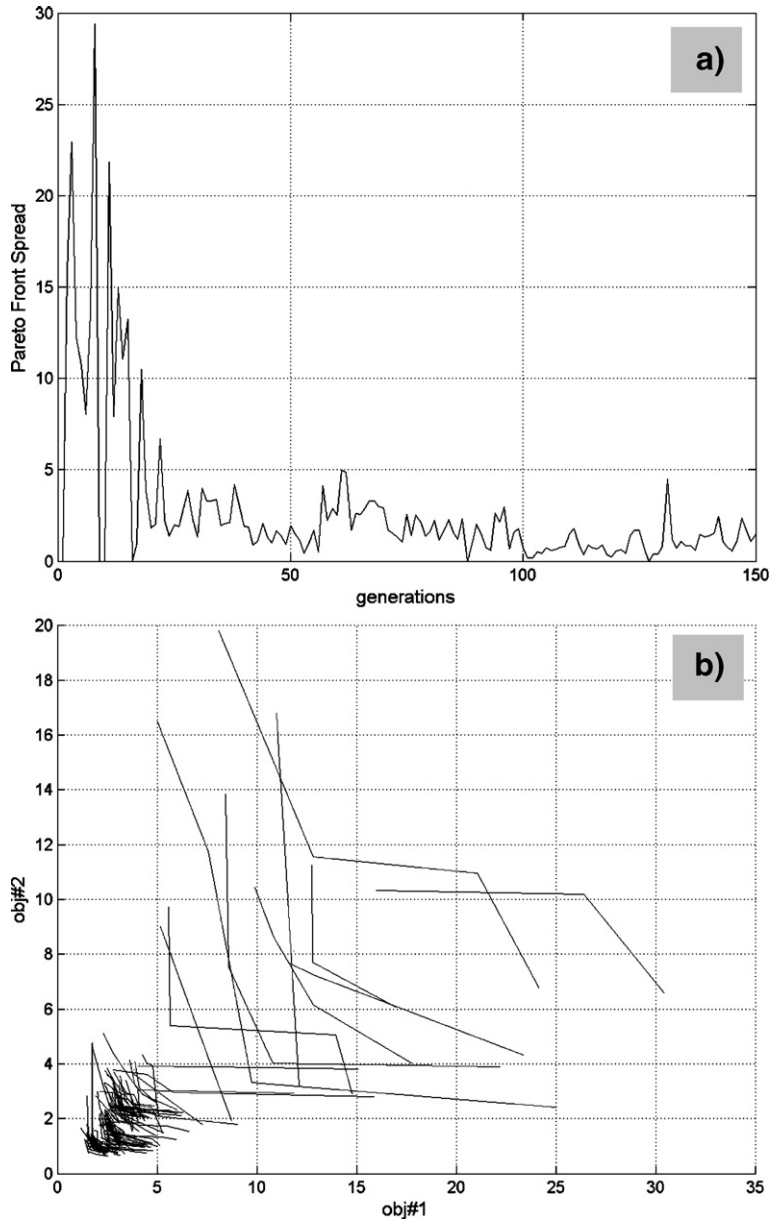

Fig. 6. Synthetic case; test#3: (a) Pareto front length over the passing generations, (b) Pareto front evolution in the objective space (darker grey as far as generations succeed).

diagonal terms of the covariance matrix (Gerstoft and Mecklenbrauker, 1998).

3.1. Synthetic cases

The method was tested for a series of synthetic cases referring to the 5-layer model presented in Fig. 2 and identified in Table 1 as model#1.

The model can be considered as a representative of a shallow unconsolidated-sediment sequence (first three layers with $V_S < 200$ m/s and a velocity inversion at the third layer) lying on a higher velocity (e.g. more compact) layer ($V_S = 400$ m/s, typical for instance of gravels) on top of a solid bedrock ($V_S = 2000$ m/s).

Because the considered sequence typically prevents from higher-mode observation, all the performed inversions were accomplished while considering only the fundamental mode (Fig. 2c).

We initially performed the data inversion while considering only the first objective (the dispersion curve misfit), then adding the second one (S-wave reflection travel time misfit) for one (test#2) and three (test#3) reflectors, to evaluate the improvement of the retrieved model while increasing the number of constraining data.

Considering the difficulties often related both with the identification and interpretation of the reflectors and with the tentative number of strata to use in the inversion procedure, we decided to perform also a series of inversions while intentionally making some wrong assumptions. The goal was the evaluation of the characteristics of the inversion results when some wrong conjecture is assumed. The entire set of tests is summarized in Table 4.

Only basic observations will be presented in the present paragraph while a thorough discussion will be offered in the next one.

The results of the first inversion (while considering only the dispersion curve, test#1) are reported in Fig. 3. In this case two final models can be defined: the one characterized by the smallest misfit (the *best* model) and a MPPD-based mean model. The similarity indices for the retrieved solutions are both close to 75% (Table 4).

Two inversions were then performed by adding the second objective (the reflection travel time misfit) for one (test#2) or three (test#3) reflectors. For test#2 we adopted the third reflector (Fig. 2) while for test#3 we included also the second and fourth ones.

For test#2, in Fig. 4 are shown the observed and calculated data, the retrieved models, the objective space and the evolution of the objectives over the passing generations (for each generation is shown the smallest obj#1 value, the corresponding obj#2 for the same model and the mean obj#1; the same values are also shown for the obj#2).

Similarity indices SIs are reported in Table 4. As for a multi-objective case no absolute *best* model can be defined, in addition to the values for the mean model are also reported the minimum and maximum values for the models belonging to the Pareto front.

For test#3 (three reflectors), Fig. 5 reports the objective space (also presented a close-up of the Pareto front with indicated approximated length), the observed and calculated data and the evolution of the objectives over the generations. For the same test Fig. 6 shows the evolution of the Pareto front. The length of the Pareto front (calculated as the sum of the distances between adjacent Pareto front models — see e.g. Fig. 5b) is plotted over the generations (showing a major decrease lowering from about 25 down to approximately 0) (Fig. 6a) and in the objective space (different grey tones in Fig. 6b).

The next four tests were performed while intentionally making some wrong assumptions in the reflector identification (tests#4 and 5), in the adopted number of strata (six instead of five, test#6) and when the models pertaining to the dispersion curve and the reflection travel times are slightly different (test#7) (see Table 4).

The first two tests (tests#4 and 5) were performed while assuming the travel times actually belonging to the fourth horizon (see Fig. 2) as if pertaining to the third or second one. Results are reported in Figs. 7 and 8. With respect to the results of tests#2 and 3 it can be noticed that the Pareto front instead of collapsing towards the origin of the coordinate system thus determining a pointy objective function distribution (see Figs. 4c and 5a), tends to spread along a front whose aperture and asymmetry with respect to the rest of the models is somehow proportional to the error of the assumed interpretation (compare Figs. 7d and 8d). The decrease of the Pareto front length is opposed by the erroneous interpretation (compare values and trends in Figs. 7f and 8f with those in Fig. 6a).

Test#6 was performed while assuming a wrong number of strata (six instead of five), still somehow properly interpreting the two reflectors adopted for the obj#2 (belonging and correctly attributed to the two deepest horizons).

Results are presented in Fig. 9. With respect to the ideal case (tests#2 and 3) it can be noticed a wider Pareto front and a fluctuating behaviour of the objectives over the generations (Fig. 9d, e and f)

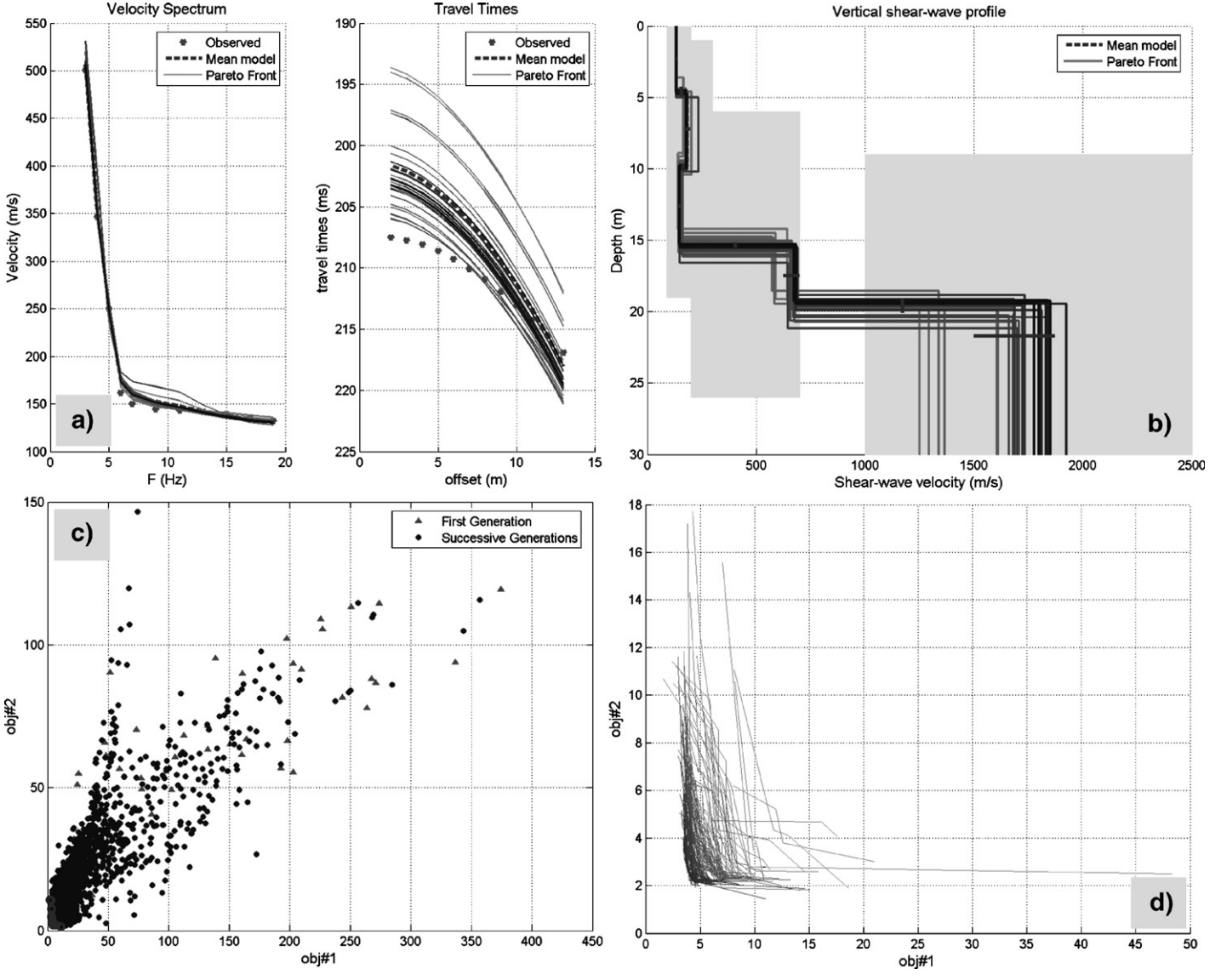

Fig. 7. Synthetic case, test#4: (a) observed and calculated data (mean and Pareto front models), (b) retrieved models, (c) objective space, (d) Pareto front evolution in the objective space over the generations (darker grey as far as generations succeed), (e) objective evolution and (f) Pareto front length over the generations.

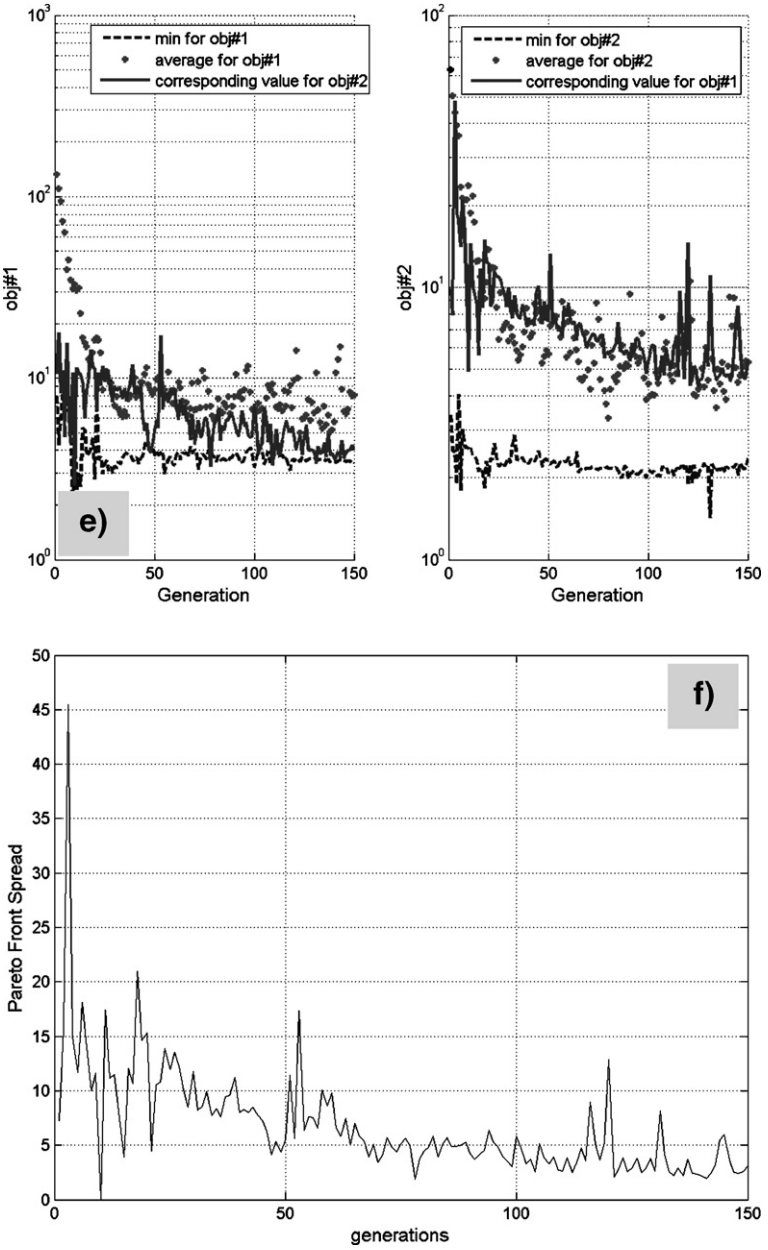

Fig. 7 (*continued*).

very likely induced by the higher degree of freedom of the system.

A final test was performed while considering the dispersion curve and travel times belonging to two slightly-different models (test#7). For the travel times we still considered model#1 while for the dispersion curve we adopted the model indicated in Table 1 as model#2.

Results in Fig. 10 show minor disturbances and fluctuations in the Pareto front evolution over the passing generations (Fig. 10d and f) and in the evolution of the objective values (Fig. 10e).

3.2. Field dataset

The proposed procedure was then used to invert a field dataset from a waste disposal site in NE-Italy (Monfalcone). A number of geophysical surveys were performed in the area, also including some boreholes

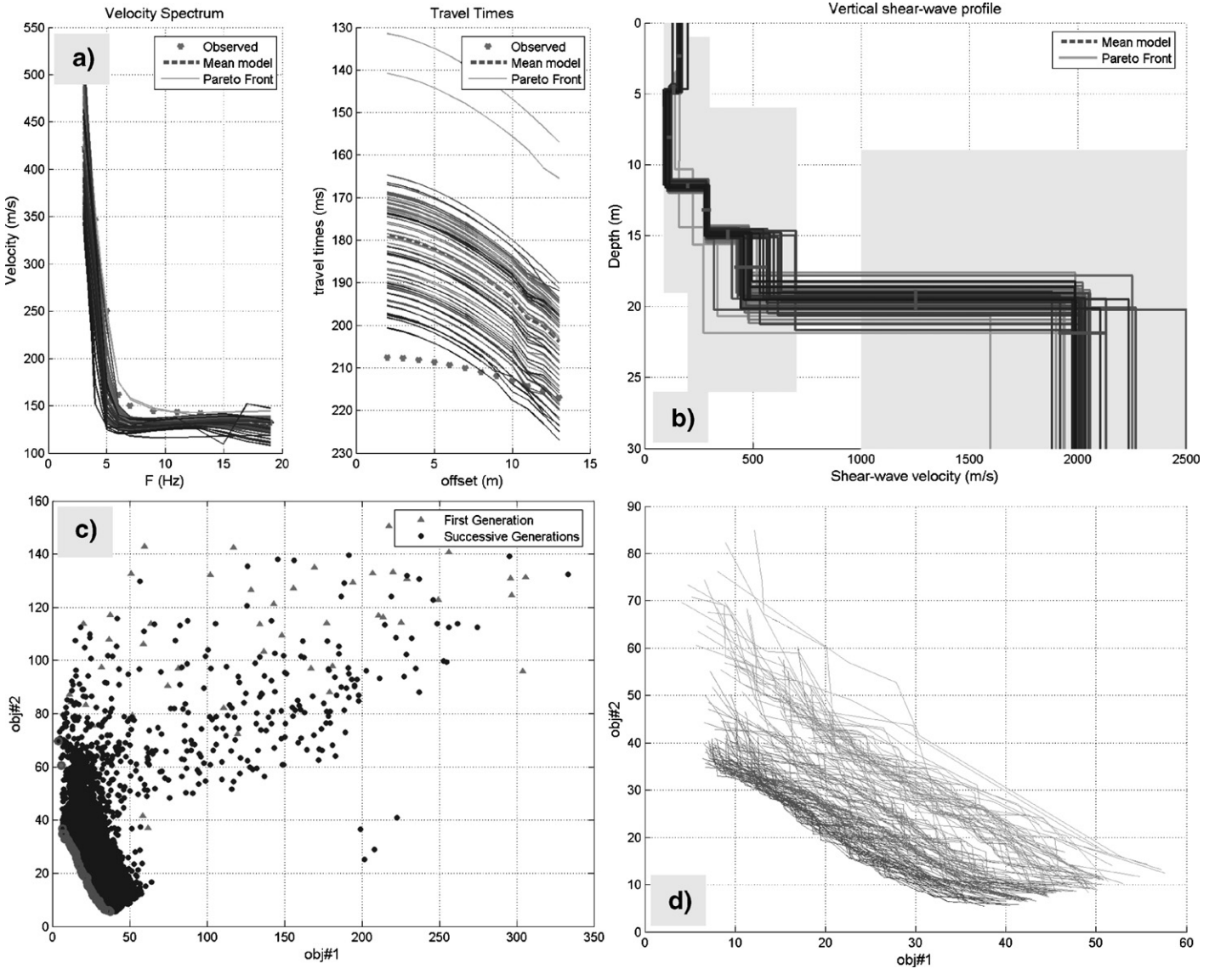

Fig. 8. Synthetic case, test#5: (a) observed and calculated data (mean and Pareto front models), (b) retrieved models, (c) objective space (d) Pareto front evolution in the objective space over the generations (darker grey as far as generations succeed), (e) objective evolution and (f) Pareto front length over the generations.

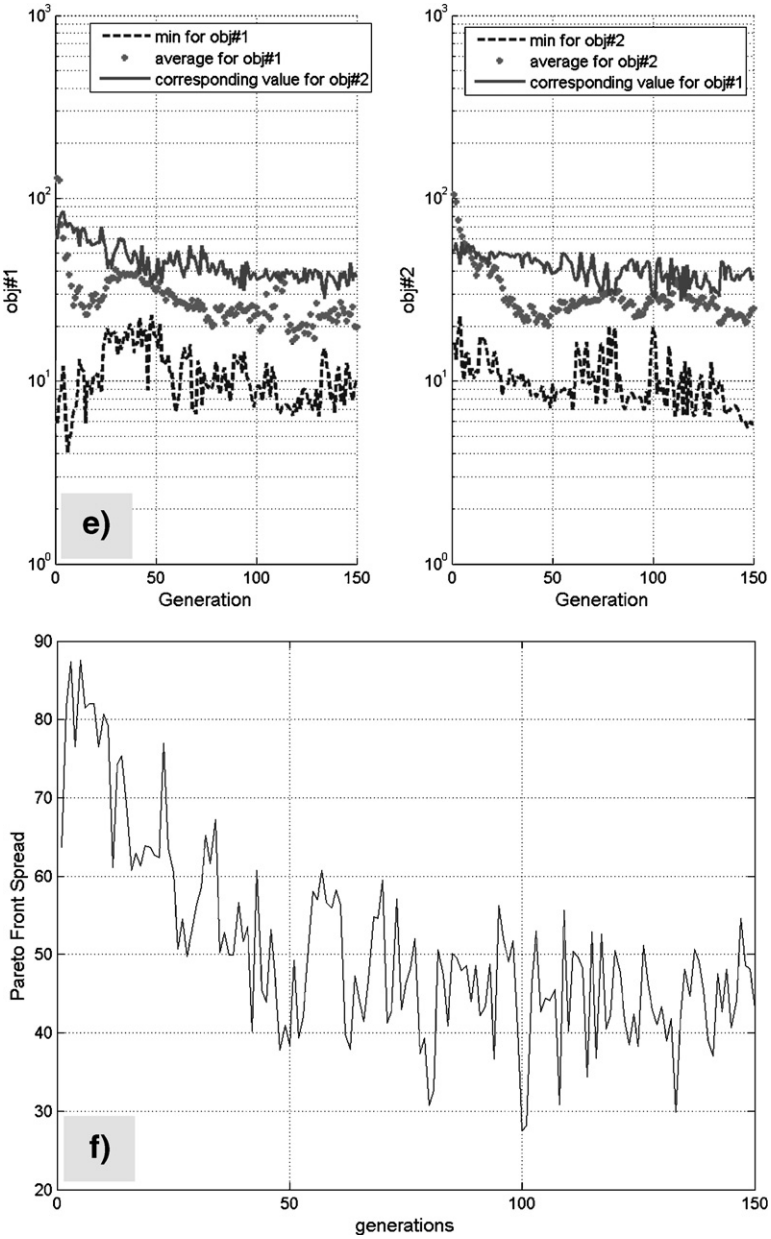

Fig. 8 (*continued*).

that put in evidence an 18 m-thick unconsolidated-sediment sequence lying on a limestone bedrock (Dal Moro et al., 2003b).

Two seismic surveys (P- and SH-wave) were accomplished according to the parameters reported in Tables 5 and 6 and data analysed also separately (Dal Moro et al., 2005). P-wave data were used for the Rayleigh wave analysis but, due to the poor geotechnical characteristics of the uppermost layers (inducing relevant attenuation effects) and the large amplitude of the surface waves, gave no evidence of any clear reflector. On the contrary, the SH-wave dataset (Fig. 11) shows a much higher signal-to-noise ratio and reveals some reflectors of which one particularly remarkable.

Fig. 12 reports a P-wave common-shot gather and the velocity spectrum calculated by means of *phase-shift* (Park et al., 1998; Dal Moro et al., 2003a). Two further dispersion curves picked for two adjacent 10 m-spaced common-shot gathers are also shown and their slightly different trends make apparent the effect of lateral variations.

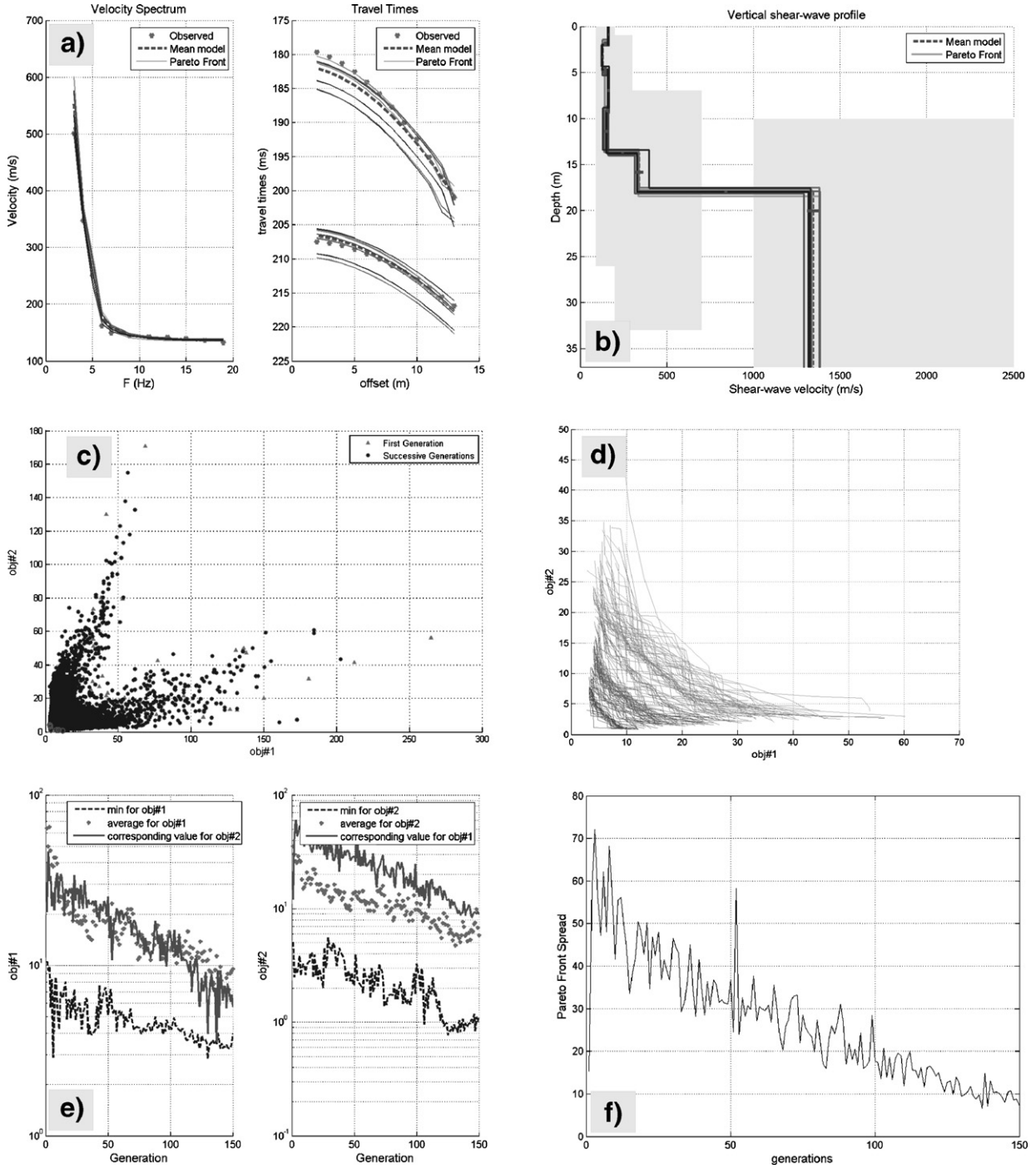

Fig. 9. Synthetic case, test#6: (a) observed and calculated data (mean and Pareto front models), (b) retrieved models, (c) objective space, (d) Pareto front evolution in the objective space over the generations (darker grey as far as generations succeed), (e) objective evolution and (f) Pareto front length over the generations.

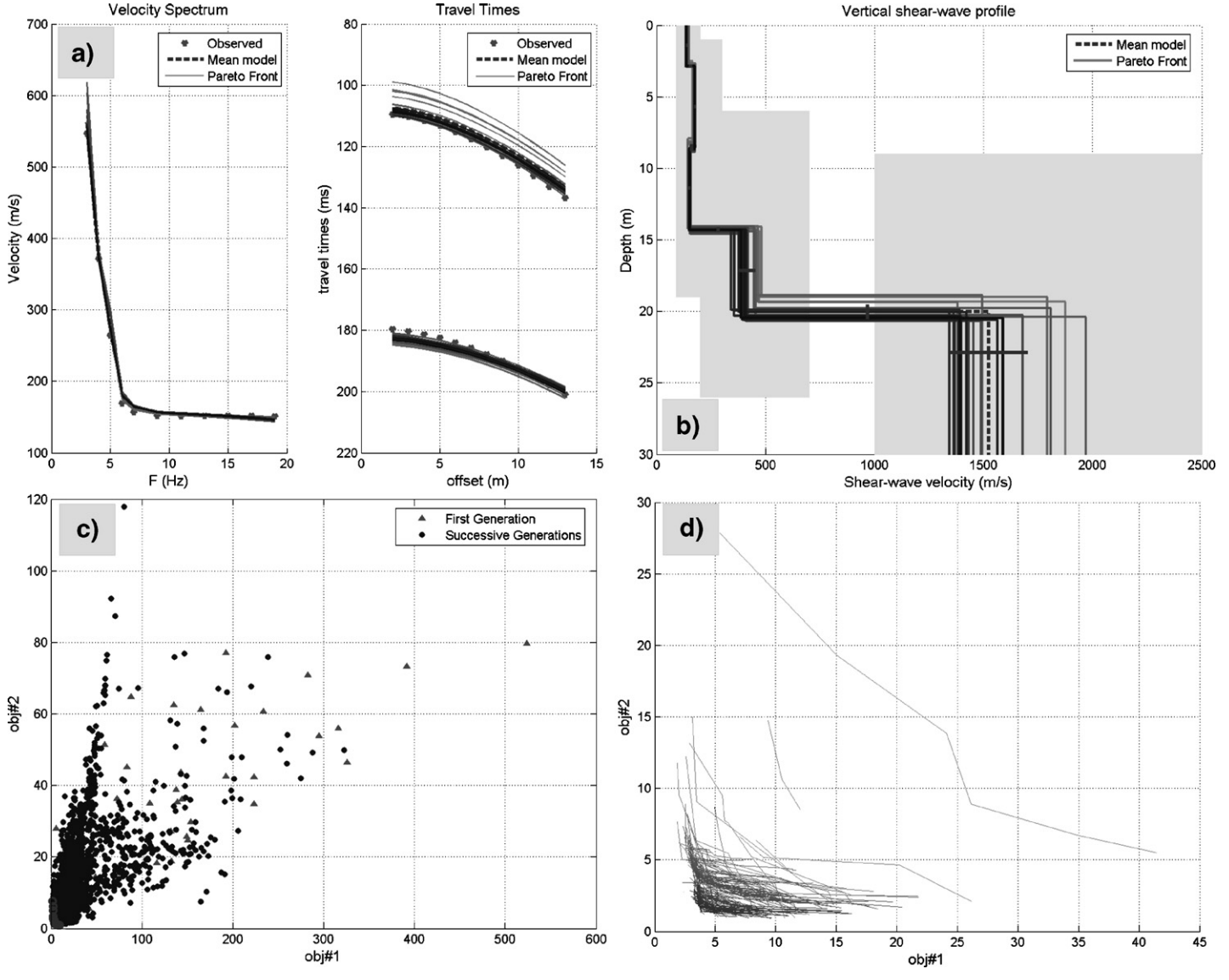

Fig. 10. Synthetic case, test#7: (a) observed and calculated data (mean and Pareto front models), (b) retrieved models, (c) objective space, (d) Pareto front evolution in the objective space over the generations (darker grey as far as generations succeed), (e) objective evolution and (f) Pareto front length over the generations.

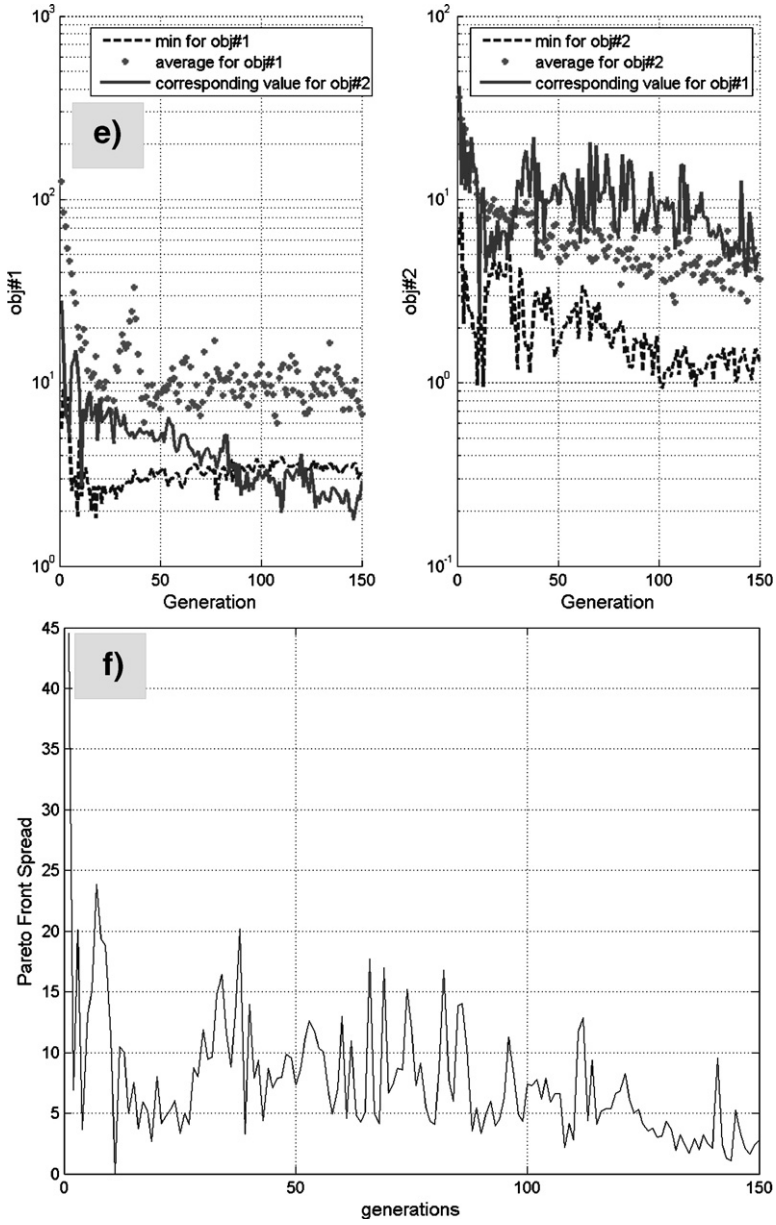

Fig. 10 (*continued*).

Two inversions were performed, both considering a 5-layer model but with two different interpretations for the picked reflection travel times (Fig. 11).

For the first inversion, similarly to the interpretation given in Dal Moro et al. (2005), such reflector was assumed as belonging to the fourth horizon (gravel-bedrock) (results are presented in Fig. 13).

A second inversion was performed while assuming that such reflection represents the silt–gravel contact (third interface in our 5-layer model) and the results are shown in Fig. 14.

While an evaluation of the results will be discussed in the next paragraph, it is useful to immediately point out the smaller misfit between the observed and calculated dispersion curves for the first inversion (Fig. 13) and the different evolution of the Pareto front and objectives over the passing generations.

4. Discussion

The joint inversion of dispersion curve and reflection travel times was considered in the framework of a bi-

Table 5
Acquisition parameters of the vertical-component survey

Source interval	5 m
Number of shots	23
Receiver spacing (24 channels)	2 m
Minimum offset	5 m
Sample interval	1 ms
Acquisition time	1 s

objective problem solved by means of an evolutionary algorithm in which the fitness is assigned on the basis of the temporary (or local) ranking of the candidate solutions.

In the previous sections we presented the results of a series of inversions performed both on a synthetic and real dataset.

A first test (test#1) was performed by considering only one objective (the dispersion curve misfit) while for the next two cases (tests#2 and 3) we considered the bi-objective case obtained by adopting travel times for one (test#2) or three reflectors (test#3).

The *Similarity Indices* (SIs) reported in Table 4 make apparent the improvement of the retrieved models while increasing the model constrains (75% when only the first objective is adopted and up to 88% for the joint inversion).

It can be noticed that for tests#2 and 3 (in which the number of layers and the horizon(s) were properly set) the Pareto front is highly symmetric (see e.g. Fig. 5a and b) and the model distribution in the objective space tends to collapse towards the utopia point [0, 0] thus determining a clear decrease in the Pareto front length over the passing generations (e.g. Fig. 6a and b).

On the other hand, when some major error in the provisional data interpretation is made (tests#4 and 5) a loss in the Pareto front symmetry is observed (e.g. Fig. 8c) and its length decrease over the generations appears modest (e.g. Fig. 8f).

It is important to remark that in this case even if the error *directly* affects only the uppermost portion of the model, as "side effect" the deeper layers will be involved as well. In fact, while the reflection misfit will be indifferent to model variations regarding deeper horizons, the dispersion curve will try to adjust the deeper layers in order to balance the erroneous uppermost structure suggested by the reflection travel times — see low *Similarity Indices* for tests#4 and 5 in Table 4.

Two further cases in which minor errors were intentionally considered (tests#6 and 7) show values and trends somehow intermediate: Pareto front symmetry seems to remain a characteristic feature but a limited and irregular decrease of the Pareto front length and objective values are observed (Figs. 9 and 10).

For the sake of clarity, the fundamental criterion to evaluate model distribution in the objective space is summarized in Fig. 15 through the schematic representation of three cases: the ideal case in which the number of strata and the reflector interpretation are properly set (Fig. 15a) (tests#2 and 3), the case of major data misinterpretations leading to severely-conflicting objectives (tests#4 and 5) (Fig. 15b) and the case of slightly-conflicting objectives due to minor errors or lateral variations (Fig. 15c) (tests#6 and 7).

The key element to evaluate the tentative provisional interpretation (number of strata and reflector identification) is given by the way the Pareto front spreads with respect to the rest of the models. In the ideal case, as the generations go by, the front maintains its symmetry and tends to collapse towards the utopia point. The length of the Pareto front (the arc AA′) tends to decrease as clearly the ratio AA′ to BB′, where B and B' represent the worst models with respect to obj#2 and obj#1, respectively. In case of only slightly conflicting objectives (tests#6 and 7), the Pareto front cannot easily collapse towards the utopia point and the decrease of the Pareto front length is limited and fluctuating. The symmetry of the Pareto front remains a characteristic feature. Lateral heterogeneities (somehow simulated by the test#7) or an inappropriate number of strata (test#6) are possible examples.

When we run into some important error in the provisional data interpretation, the model distribution in the objective space suffers from major deformations (see e.g. Fig. 8c) and there is a loss of symmetry between the Pareto front and the rest of the models (Fig. 15b and tests#4 and 5 in Figs. 7 and 8).

A further feature is the evolution of the objective values over the passing generations. When the tentative data interpretation is correct (tests#2 and 3) both objectives tend to decrease (as well as the average value) (see Figs. 4d and 5d). On the other side, important errors in the inversion setting induce fluctuating or flat trends (tests#4 and 5 in Figs. 7e and 8e), typically vaguer

Table 6
Acquisition parameters of the SH-wave survey

Source interval	1 m
Receiver interval	1 m
Number of channels	12
Minimum offset	2 m
Number of shots	24
Vertical stack	4
Acquisition configuration	Off-end shooting

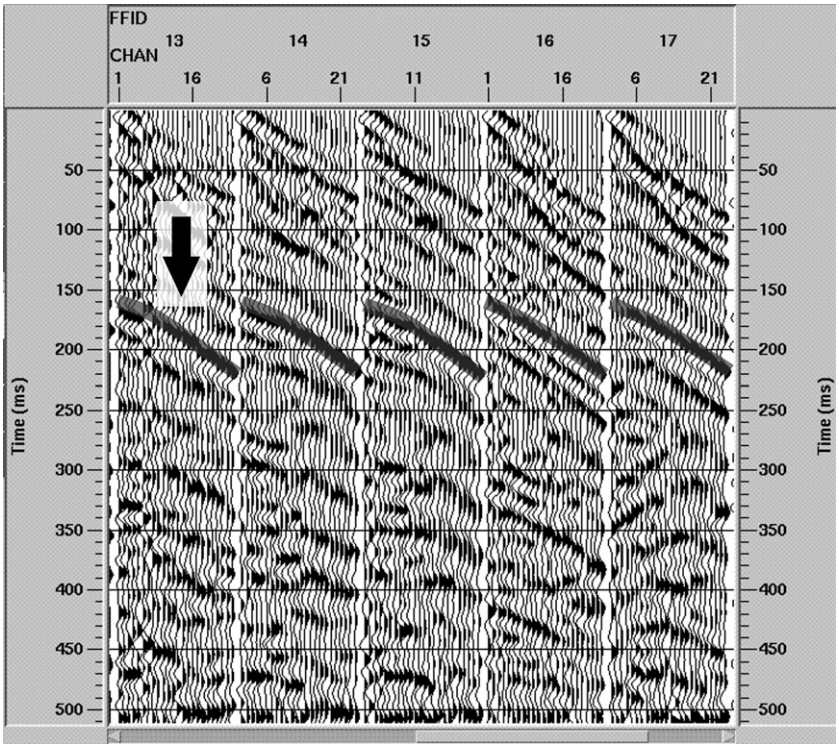

Fig. 11. SH-wave survey: five common-shot gathers. In evidence the reflector used for the joint inversion.

in case of smaller interpretative mistakes (tests#6 and 7 in Figs. 9e and 10e).

When compared with the results obtained for the synthetic cases, values and trends of the field dataset (Figs. 13 and 14) support the hypothesis of minor discrepancies that we speculate to be related to lateral heterogeneities in the investigated area.

It is in fact well-known that one of the main problems in surface wave analysis pertains to the effect of lateral heterogeneities that reduce the resolution of the survey. MASW (Multi-channel Analysis of Surface Wave) technique requires in fact long arrays that, due to lateral variations, will eventually mirror in unfocused velocity spectra or split modes. Techniques

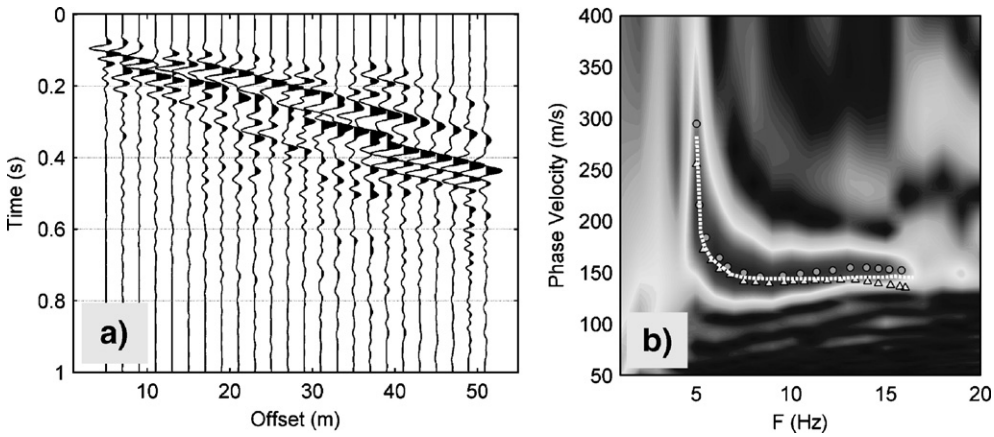

Fig. 12. P-wave survey: (a) common-shot gather, (b) corresponding velocity spectrum used for the inversion. The circles represent the dispersion curve of the considered common-shot while the triangles and the dotted line depict the dispersion curves picked from two adjacent (10 and 20 m distance) common-shot gathers.

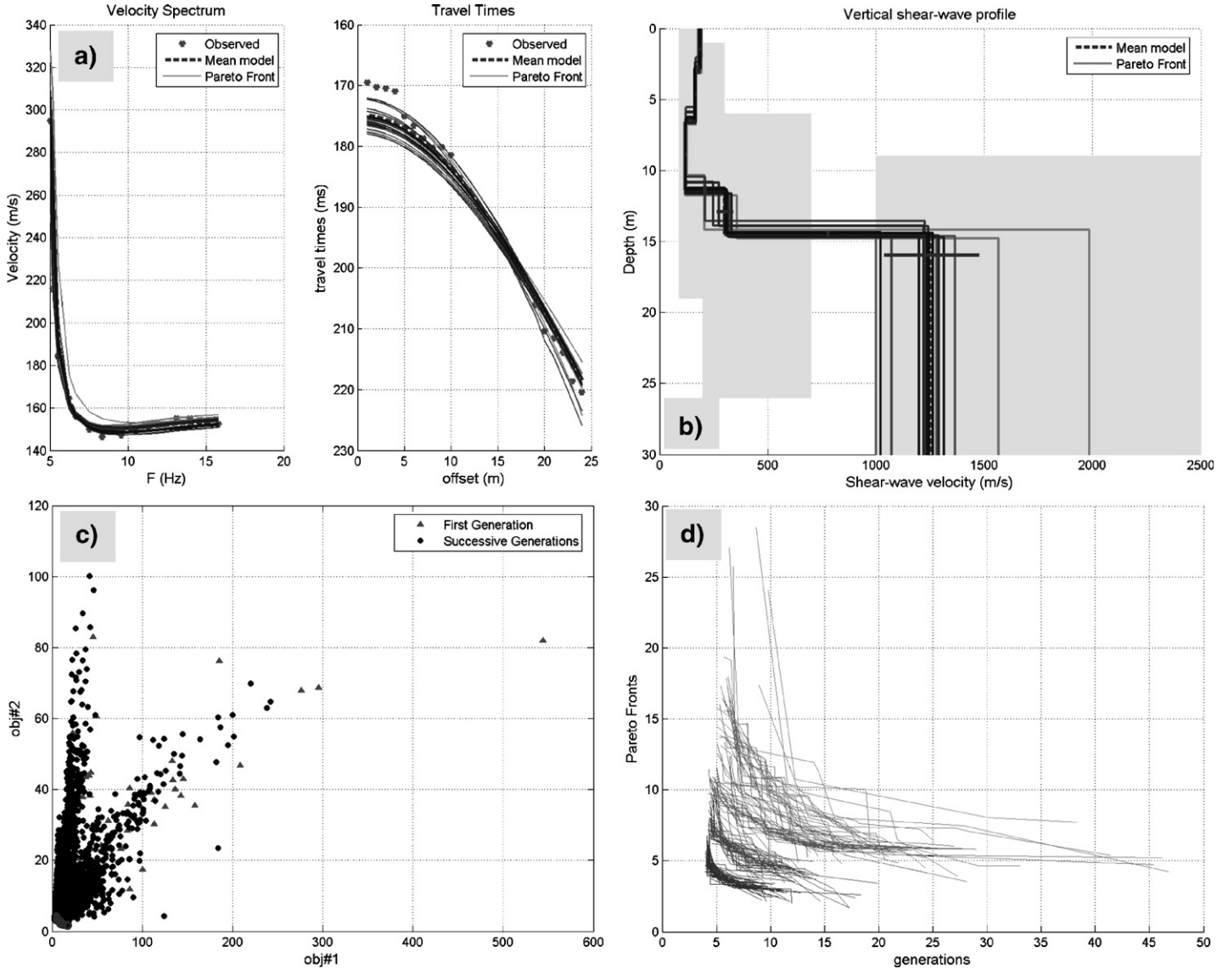

Fig. 13. Real dataset: results of the inversion performed when assuming that the reflector evidenced in Fig. 11 pertains to the forth interface: (a) observed and calculated data (mean and Pareto front models), (b) retrieved models, (c) objective space, (d) Pareto front evolution in the objective space over the generations (darker grey as far as generations succeed), (e) objective evolution and (f) Pareto front length over the generation.

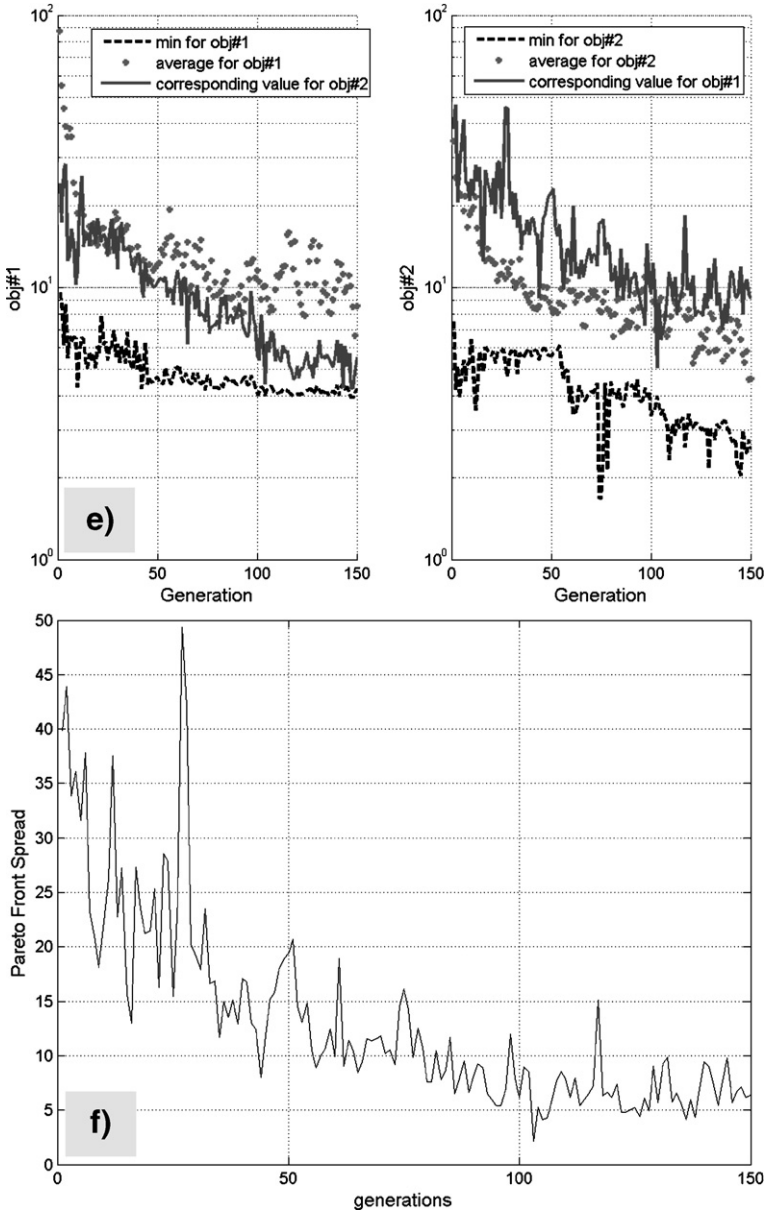

Fig. 13 (*continued*).

based on Common Mid-Point (CMP) gathers have been proposed in order to reduce these problems by Shtivelman (2002) and Hayashi and Suzuki (2004).

Because of the length of the geophone arrays the dispersion curve and the reflection travel times can refer to two slightly-different average models. As for the field dataset considered in this work, the travel times can typically refer to a 22 m geophone array while the dispersion curve are determined while considering a length of 46 m (if then we consider the distance between the source and the last geophone these values increase respectively to 24 and 51 m — Tables 5 and 6).

The analyses of the field dataset reveal some interesting aspect. In fact, according to the paradigms suggested by the evaluation of the synthetic cases, the inversion presented in Fig. 13 (the observed reflection is attributed to the fourth interface of the 5-layer model) seems to be preferable to the one presented in Fig. 14 (where the reflection is assumed to belong to the third interface). The resulting final models are quite different: one proposes the bedrock at about

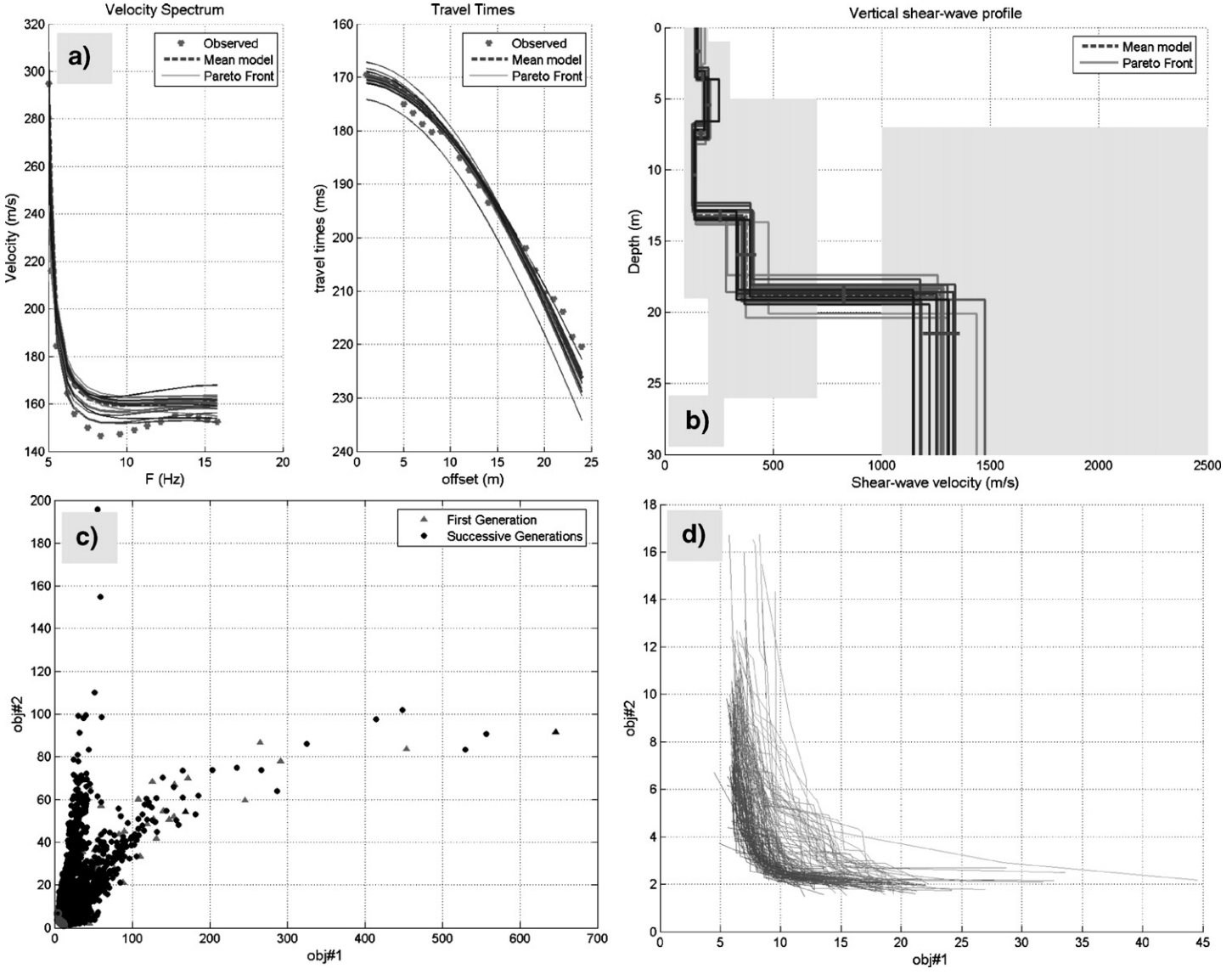

Fig. 14. Real dataset: results of the inversion performed when assuming that the reflector evidenced in Fig. 11 pertains to the third interface: (a) observed and calculated data (mean and Pareto front models), (b) retrieved models, (c) objective space, (d) Pareto front evolution in the objective space over the generations (darker grey as far as generations succeed), (e) objective evolution and (f) Pareto front length over the generations.

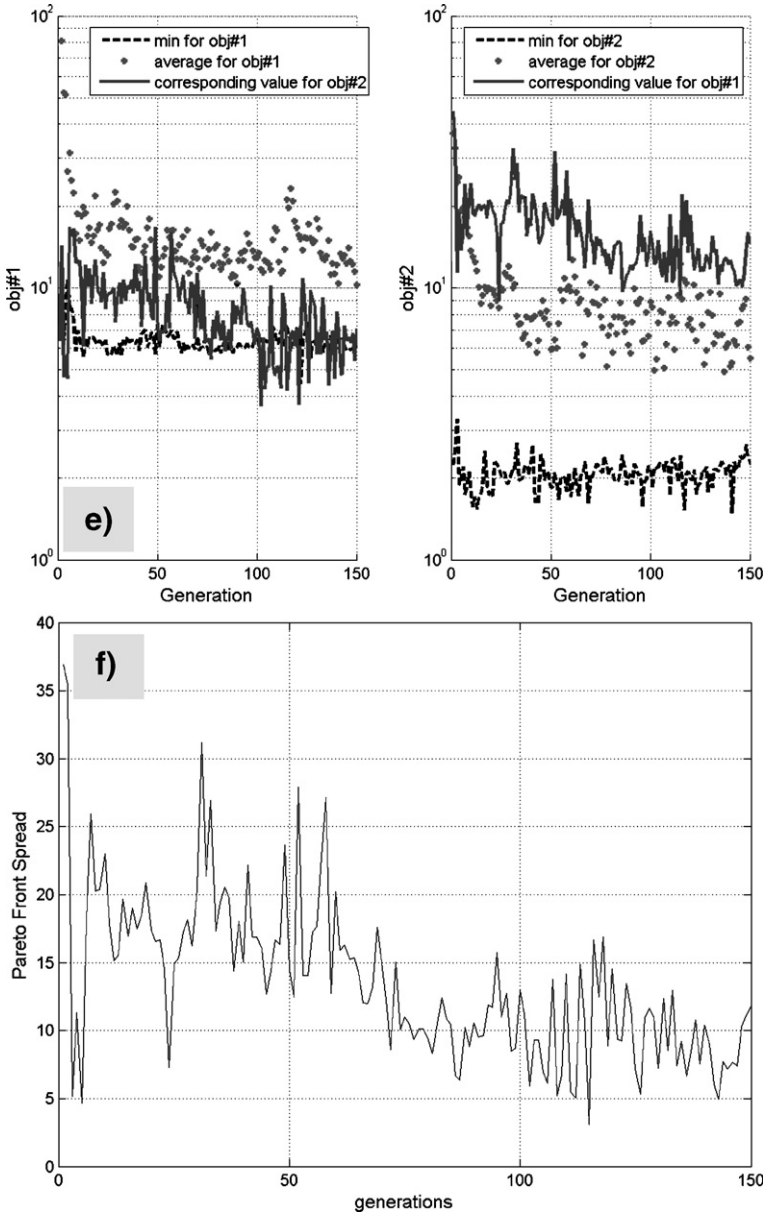

Fig. 14 (*continued*).

15 m (Fig. 13), while the other at about 18 m (Fig. 14).

On the other hand, the stratigraphy of a borehole drilled about 5 m apart from the source position of the considered common-shot gather (so about 30 m from the mid-point of the P-wave array) indicates the limestone bedrock at about 18 m, while outcrops are present about 40–50 m from the survey line and perpendicular to it thus giving evidence a remarkably-complex bedrock topography.

Hence, the geological evidence and the comparison of the real-data inversion with the synthetic cases suggest lateral variations and/or azimuthal anisotropies as possible causes for the observed features. A perpendicular seismic survey would probably help to gain further insights into the investigated area.

5. Conclusions

The main motivation of the present work lies on the observation that the inversion of surface wave dispersion curve is a very hard task both for linear and global-search methods and further aspects of the seismic wave field

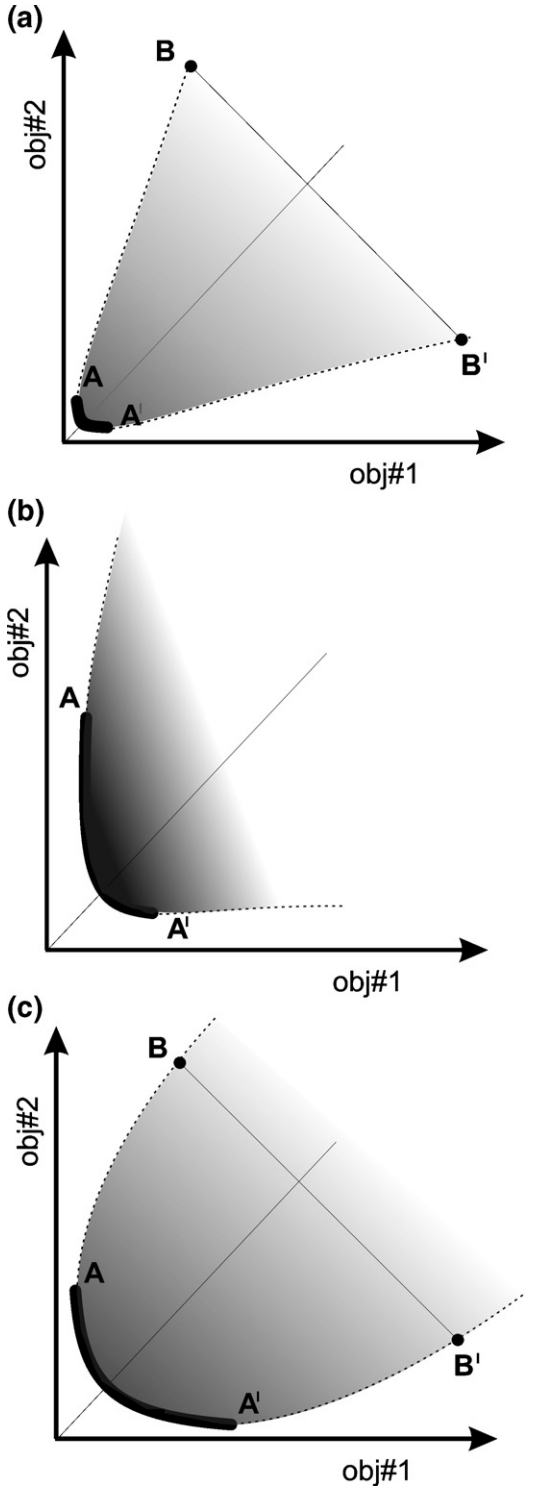

Fig. 15. Model distribution in the objective space for three fundamental cases: (a) ideal case (tests#2 and 3), (b) severely-conflicting objectives (tests#4 and 5), (c) slightly-conflicting objectives (tests#6 and 7).

should be considered to better constrain the inversion and overcome the severe indeterminacy of the solution determined by dispersion curve analysis only.

In spite of the fact that in the last decade surface wave analysis has been receiving a primary interest for shallow vertical shear-wave profiling, minor efforts were dedicated to improve the robustness and reliability of the inversion procedure. This is a general problem in geophysical-data inversion and can become highly problematic in the specific case, particularly when dealing with unconsolidated-sediment cover and a sledgehammer source that determine fundamental mode dispersion curve lacking of higher frequencies thus sometimes unable to constrain a good final solution.

In the present work a joint inversion of Rayleigh wave dispersion curve and reflection travel times is performed according to a bi-objective evolutionary algorithm based on a ranking system determined according to the dominance criterion.

For the second objective (reflection travel time misfit) we considered shear-wave data both for the usually good signal-to-noise ratio (e.g. Guy et al., 2003; Dal Moro et al., 2005) and because of the tighter link with the character of the Rayleigh wave propagation, that is mainly function of V_S rather than V_P (e.g. Xia et al., 1999).

The method can be modified by using or adding other objectives and considerations analogues to those depicted in the previous sections can be adopted in order to evaluate the inversion results. A paper dealing with the joint inversion of the dispersion curves and refraction travel times will be shortly submitted by the authors.

Unlike single-objective optimizers obtainable by means of an arbitrary summation of two or more objectives, the present approach allows to properly handle the *non-commensurable* nature of the two objectives and provides important indications about the tentative interpretations inherently assumed in the inversion process (number of strata and reflection horizon identification).

In shallow reflection surveys data interpretation can be particularly problematic. In the processed sections, refractions and airwaves can be misinterpreted as reflections and processing artefacts can appear (Steeples and Miller, 1998). The described methodology is useful not only to better constrain the inversion but also to help the interpretation of the reflections with respect to the structure (number of strata).

A series of synthetic tests were performed and enabled us to verify a significant improvement of the

retrieved model as long as we add more constrains (the reflection travel times used for the second objective).

Furthermore, the ensemble of inversion outputs also provides some criteria to evaluate the consistency of the overall inversion process.

Model distribution and Pareto front spread in the objective space and over the passing generations (as well as the coherent decrease of the two objectives over the generations) were identified as good indicators to assess the consistency of the performed inversion (depending on the provisional data interpretation inherently adopted).

In the light of the considered synthetic tests, the results of the analyses performed on a field dataset were evaluated as possible evidence of lateral heterogeneities.

Acknowledgements

This research was supported by CNR (The Italian National Research Council), National Group for defense against chemical, industrial and ecological hazards, grant no. 00.00623.PF37 and by the European contract EVK4-CT-2001-00046, HYGEIA.

Part of the work was performed during a stay of one of the authors (Giancarlo Dal Moro) at the *Institute of Hydrogeology, Engineering Geology and Applied Geophysics* (Faculty of Science, Charles University, Prague- CZ). The stay was supported by a CNR – NATO (North Atlantic Treat Organization) advanced fellowship. The authors would like to express their gratitude to the Director of the Department, Prof. Jan Vilhelm, for his kind support and to Paolo Gabrielli (from DiSGAM) for providing the reflection travel times of the Monfalcone dataset and for his continuous sympathetic and cooperative spirit.

References

AAVV, CREWES Project, 2001, open file, www.crewes.ucalgary.ca/Samples/EduSoftware/.

Adme, Z.G., 2004. Analysis of NATM Tunnel Responses due to Earthquake Loading in Various Soils. REUJAT (Research Experiences for undergraduates in Japan in Advanced Technology) 2004. open file, http://wusceel.cive.wustl.edu/reujat/2004/adme.pdf.

Coello Coello, C.A., 2002. Evolutionary Multiobjective Optimization: Past, Present and Future. Open file, http://www.cs.cinvestav.mx/~EVOCINV/download/tutorial-moea.pdf.

Coello Coello, C.A., 2003. Guest editorial: special issue on evolutionary multiobjective optimization. IEEE Transactions on Evolutionary Computation 7, 97–99.

Dal Moro, G., Pipan, M., Forte, E., Finetti, I., 2003a. Determination of Rayleigh Wave Dispersion Curves for Near Surface Applications in Unconsolidated Sediments. Proceedings SEG 2003, 73rd Annual Meeting, Dallas, Texas, 26–31 October 2003.

Dal Moro, G., Pipan, M., Forte, E., Sugan, M., Finetti, I., 2003b. Integrated non-invasive characterization of waste disposal site. Proceedings Symposium EEGS 2003 (Environmental and Engineer Geophysical Society), Prague, (Czech Republic), August 31–September 4 2003, O-085.

Dal Moro, G., Pipan, M., Forte, E., Gabrielli, P., Sugan, M., Forlin, E., Finetti, I., 2005. Shear-Wave Profiling via SH Reflection Analysis and Rayleigh Wave Inversion. Extended Abstract SEG 2005, 75th Annual Meeting, Houston, Texas, 6–11 November 2005. available on-line at http://seg.org, link "SEG Technical Program Expanded Abstracts".

Dal Moro, G., Forte, E., Pipan, M., Sugan, M., in press-a. Velocity Spectra and Seismic Signal Identification for Surface Wave Analysis. Near-Surface Geophysics.

Dal Moro, G., Pipan, M., Gabrielli, P., 2006. Rayleigh Wave Dispersion Curve Inversion via Genetic Algorithms and Marginal Posterior Probability Density Estimation. Geophysics 61, 39–55. doi:10.1016/j.appgeo.2006.04.002.

Fonseca, C.M., Fleming, P.J., 1993. Genetic Algorithms for Multiobjective Optimization: Formulation, Discussion and Generalization. Proceeding of the fifth International Conference on Genetic Algorithms, San Mateo, CA (USA). Morgan-Kauffman, pp. 416–423.

Frazer, L.N., Basu, A., 1990. Freeze bath inversion. Proceedings of the Sixtieth Annual International Meeting of the Society of Exploration Geophysicists (SEG). Expanded Abstracts II, 1123–1125.

Gardner, G.H.F., Gardner, L.W., Gregory, A.R., 1974. Formation velocity and density — the diagnostic basic for stratigraphic trap. Geophysics 39, 770–780.

Gerstoft, P., Mecklenbrauker, C.F., 1998. Ocean acoustic inversion with estimation of a posteriori probability distributions. Journal of the Acoustical Society of America 104, 808–819.

Glangeaud, F., Mari, J., Lacoume, J.-L., Mars, J., Nardin, M., 1999. Dispersive seismic waves in geophysics. European Journal of Environmental and Engineering Geophysics 3, 265–306.

Goldberg, D.E., 1989. Genetic Algorithms in Search, Optimization, and Machine Learning. Addison-Wesley Publishing Company, Inc. 412 pp.

Guy, E.D., Nolen-Hoeksema, R.C., Daniels, J.J., Lefchik, T., 2003. High-resolution SH-wave seismic reflection investigations near a coal mine-related roadway collapse feature. Journal of Applied Geophysics 54, 51–70.

Hayashi, K., Suzuki, H., 2004. CMP cross-correlation analysis of multi-channel surface-wave data. Exploration Geophysics 35, 7–13.

Ivanov, J., Park, C.B., Miller, R.D., Xia, J., 2000. Mapping Poisson's Ratio of unconsolidated materials from a joint analysis of surface-wave and refraction events. Proceedings of the Symposium on the Application of Geophysics to Engineering and Environmental Problems (SAGEEP 2000), Arlington, Va., February 20–24, pp. 11–19.

Lai, C.G., Rix, G.J., 1998. Simultaneous Inversion of Rayleigh Phase Velocity and Attenuation for Near-Surface Site Characterization. Georgia Institute of Technology, School of Civil and Environmental Engineering, Report No. GIT-CEE/GEO-98-2, July, 1998. 258 pp.

Man, K.F., Tang, K.S., Kwong, S., 2001. Genetic Algorithms. Springer. 344 pp.

Park, C.B., Xia, J., Miller, R.D., 1998. Imaging dispersion curves of surface waves on multichannel record. Proceedings SEG 1998, 68th Ann. Internat. Mtg., Soc. Explor. Geophys., Expanded Abstracts, pp. 1377–1380.

Park, C.B., Miller, R.D., Xia, J., 1999. Multichannel analysis of surface waves. Geophysics 64, 800–808.

Ritzwoller, M.H., Lavshin, A.L., 2003. Estimating shallow shear velocities with marine multicomponent seismic data. Geophysics 67, 1991–2004.

Sen, M.K., Stoffa, P.L., 1992. Rapid sampling of model space using genetic algorithms: examples from seismic waveform inversion. Geophysics 108, 281–292.

Shtivelman, V., 2002. Surface wave sections as a tool for imaging subsurface inhomogeneities. European Journal of Environmental and Engineering Geophysics 7, 121–138.

Steeples, D.W., Miller, R.D., 1998. Avoiding pitfalls in shallow seismic reflection surveys. Geophysics 63, 1213–1224.

Stoffa, P.L., Sen, M.K., 1991. Nonlinear multiparameter optimisation using genetic algorithms: inversion of plane wave seismograms. Geophysics 56, 1794–1810.

Tatham, R.H., McCormack, M.D., 1991. Investigations in Geophysics no. 6, Multicomponent Seismology in Petroleum Exploration. In: Neitzel, E.B., Winterstein, D.F. (Eds.), Society of Exploration Geophysicists, Tulsa. 248 pp.

Van Veldhuizen, D.A., Lamont, G.B., 1998a. Multiobjective Evolutionary Algorithms: A History and Analysis. Air Force Institute of Technology. Technical Report TR-98-03. 88 pp.

Van Veldhuizen, D.A., Lamont, G.B., 1998b. Evolutionary Computation and Convergence to a Pareto Front. In: Koza, John R. (Ed.), Late Breaking Papers at the Genetic Programming 1998 Conference. Stanford University, pp. 221–228.

Van Veldhuizen, D.A., Lamont, G.B., 2000. Multiobjective Evolutionary Algorithms: Analyzing the State-of-the-Art. Evolutionary Computation 8, 125–147.

Whidborne, J.F., Gu, D.W., Postlethwaite, I., 1994. MODCONS — a MATLAB Toolbox for Multi-Objective Control System Design. Open file, http://www.eee.kcl.ac.uk/mecheng/jfw/modcons.html.

Woods, R.D., 1968. Screening of surface waves in soils. Journal of Soil Mechanics and Foundations Division, ASCE 94, 951–979.

Xia, J., Miller, R.D., Park, C.B., 1999. Estimation of near-surface shear-wave velocity by inversion of Rayleigh waves. Geophysics 64, 691–700.

Xia, J., Miller, R.D., Park, C.B., Tian, G., 2003. Inversion of high frequency surface waves with fundamental and higher modes. Journal of Applied Geophysics 52, 45–57.

Xia, J., Miller, R.D., Park, C.B., Ivanov, J., Tian, G., Chen, C., 2004. Utilization of high-frequency Rayleigh waves in near-surface geophysics. The Leading Edge 23, 753–759.

Zitzler, E., Thiele, L., 1999. Multiobjective evolutionary algorithms: a comparative case study and the strength Pareto approach. IEEE Transactions on Evolutionary Computation 3, 257–271.